Photochemical & Photobiological Sciences

Accepted Manuscript

This is an *Accepted Manuscript*, which has been through the Royal Society of Chemistry peer review process and has been accepted for publication.

Accepted Manuscripts are published online shortly after acceptance, before technical editing, formatting and proof reading. Using this free service, authors can make their results available to the community, in citable form, before we publish the edited article. We will replace this *Accepted Manuscript* with the edited and formatted *Advance Article* as soon as it is available.

You can find more information about *Accepted Manuscripts* in the Information for Authors.

Please note that technical editing may introduce minor changes to the text and/or graphics, which may alter content. The journal's standard Terms & Conditions and the Ethical guidelines still apply. In no event shall the Royal Society of Chemistry be held responsible for any errors or omissions in this *Accepted Manuscript* or any consequences arising from the use of any information it contains.

ROYAL SOCIETY OF CHEMISTRY

www.rsc.org/pps

Title: Energy metabolism targeted drugs synergize with photodynamic therapy to potentiate breast cancer cell death

Authors: **Xiaolan Feng, Yi Zhang, Pan Wang, Quanhong Liu, Xiaobing Wang***

Affiliation: All authors are from Key Laboratory of Medicinal Resources and Natural Pharmaceutical Chemistry, Ministry of Education, National Engineering Laboratory for Resource Developing of Endangered Chinese Crude Drugs in Northwest of China, College of Life Sciences, Shaanxi Normal University, Xi'an, Shaanxi, China.

Corresponding author: Xiaobing Wang, Key Laboratory of Medicinal Resources and Natural Pharmaceutical Chemistry, Ministry of Education, National Engineering Laboratory for Resource Developing of Endangered Chinese Crude Drugs in Northwest of China, College of Life Sciences, Shaanxi Normal University, Xi'an 710062, Shaanxi, China.

E-mail: Xiaobing Wang, wangxiaobing@snnu.edu.cn

Telephone: +86-029-85310275

Energy metabolism targeted drugs synergize with photodynamic therapy to potentiate breast cancer cell death

Abstract: Malignant cells are highly dependent on aerobic glycolysis, which differs significantly from normal cells (Warburg effect). Interference of this metabolic process has been considered as an innovative method for developing selective cancer therapy. Recent study demonstrates glycolysis inhibitor 2-deoxyglucose (2-DG) can potentiate PDT efficacy, whereas the possible mechanisms haven't been carefully investigated. This study firstly proved the general potentiation of PDT efficacy by 2-DG and 3-bromopyruvate (3-BP) on human breast cancer MDA-MB-231 cells, and carefully elucidated the underlying mechanism in the process. Our results showed both 2-DG and 3-BP could significantly promote a PDT-induced cell cytotoxic effect when compared with either monotherapy. Synergistic potentiation of mitochondria- and caspase-dependent cell apoptosis were observed, including mitochondrial membrane potential (MMP) drop, Bax translocation, caspase-3 activation. Besides, ROS generation and the expression of oxidative stress related proteins such as P38 MAPK phosphorylation and JNK phosphorylation were notably increased after the combined treatment. Moreover, when pretreated with ROS scavenger N-acetylcysteine (NAC), the ROS generation, MMP drop, cell apoptosis and cytotoxicity were differently relieved, suggesting ROS was vertical in the pro-apoptotic process induced by 2-DG/3-BP combined with PDT treatment. These results indicate that by combination with glycolytic antagonists and PDT may be a promising therapeutic strategy to effectively kill cancer cells.

Keywords: Photodynamic therapy; 2-deoxyglucose; 3-bromopyruvate; apoptosis; MDA-MB-231 cells.

1. Introduction：

The significant difference between malignant cells and normal cells is cellular metabolism. Normal cells rely on oxidative phosphorylation to produce ATP, while cancer cells mainly depend on glycolysis, even in the presence of sufficient oxygen (Warburg effect).[1,2] In view of that, interference of glycolysis has become an emerging strategy for developing new selective cancer therapies.[3-5] Hexokinase -2 (HK -II), a key enzyme of glycolytic process, is the predominant form of hexokinases in cancer cells and attaches to the outer membrane of the mitochondria.[6] Inhibition HK-II can not only reduce the energy supply, but also impair mitochondria.[7] Several HK -II inhibitors, such as 2-deoxyglucose (2-DG) and 3-bromopyruvate (3-BP), have been clinically used as anticancer drugs.[8] They can disrupt the cancer metabolism system and elevate cellular ROS level eventually leading to cell death.[9] Although 2-DG suppresses cell growth in vitro, the implementation of 2-DG as an anticancer agent in vivo has been a disappointment because of its systemic toxicity.[10] 3-BP, an alkylating agent which can interact with many molecules in cells，also produces significant side effect.[11] In view of that, the clinical application of glycolysis inhibitors was somewhat limited, and the potential combinations of glycolytic inhibitors and some other curative protocols have been a promising option in cancer treatment.[12, 13]

Photodynamic therapy (PDT) is a novel approach for cancer treatment. It is based

on a photosensitizer that is activated by light with appropriate wavelength to produce reactive oxygen species (ROS), predominantly singlet oxygen, and eventually eradicate cancer cells.[14] PDT has been widely used to cure various cancers, such as breast, head, neck, skin and so on.[15] But, PDT efficacy is still limited by many factors such as sensitizer itself, light penetration ability, and so on.[16] Therefore, the combinations of PDT with some chemotherapeutic drugs have undoubtedly become an attractive approach to cancer therapy. [17, 18]

Recently, an adjunctive treatment of 2-DG and PDT has exhibited a potentiated efficacy when compared with either monotherapy,[19] but the underlying mechanism remains unclear. The present study was to investigate the general potentiation of PDT efficacy by 2-DG/3-BP on MDA-MB-231 cells, then further to carefully elucidate the underlying mechanism in the process.

2.1. Chemicals and regents

Chlorin e6 (Ce6, purity > 95 %), 2-DG and 3-BP were purchased from Sigma Chemical Company (St Louis, MO, USA). They were dissolved in sterilized PBS (0.1 M, pH 7.4) at a stock concentration of 4.19 mM, 1 M and 100 mM at -20 ℃, respectively.

N-acetylcysteine (NAC) and Rodamine 123 (RHO 123) were purchased from Sigma Chemical Company (St Louis, MO, USA). 2',7'-dichlorofluorescein diacetate (DCFH-DA) and Mito Tracker Green (MTG) were supplied by Molecular Probes Inc (Invitrogen, CA, USA). Immunoglobulin FITC or TRITC conjugates were purchased

from Beijing Zhongshan Golden Bridge Biotechnology Co., Ltd. Bax, Bcl-2, Phosphorylated-P38 MAPK, Phosphorylated-JNK and caspase-3 antibodies were from Cell Signaling Technology (Beverly, MA, USA). β-actin antibody was acquired from Santa Cruz Biotechnology (Santa Cruz, CA). All other reagents were analytical grade.

2.2. Cell culture

Human breast cancer MDA-MB-231 cells and Heart and Umbilical Vein Endothelial cells (HUVEC) were obtained from the cell bank of Chinese Academy of Science, Shanghai, China, and cultured in Dulbecco's Modified Eagle's Medium (DMEM, Sigma, St. Louis, MO) supplemented with 10% fetal bovine serum (Life Technologies, Carlsbad, CA). The cells were incubated at 37 ℃ in humidified atmosphere with a 5 % CO2 incubator. Cells in the exponential phase of growth were used in each experiment.

2.3 Photodynamic treatment

Cells were incubated with different concentrations of Ce6 for 4 h, and then exposed to light. The semiconductor laser (excitation wavelength: 650 nm; manufacturer: Institute of Photonics & Photon Technology, Department of Physics, Northwest University, Shaanxi, China) was used as a source for evocation of the PDT effect. The total light dose of 1.2 J/cm^2 was applied in the present study.

2.4 Experiment protocol

MDA-MB-231 cells and HUVEC were seeded on a 35-mm culture dish. After reaching around 70 % confluences, cells were divided randomly into six groups: (i) Control, (ii) 2-DG alone treatment, (iii), 3-BP alone treatment, (iv) PDT treatment, (v) 2-DG combined with PDT treatment (2-DG+PDT), (vi) 3-BP combined with PDT treatment (3-BP+PDT). For all groups except control and 2-DG/3-BP alone, cells were incubated with 1 μg/ml Ce6 for 4 h to allow sufficient time for cellular uptake of the photosensitizer, then exposed to 1.2 J/cm^2 laser light. Instead of Ce6, an equivalent quantity of DMEM was used for the control. For 2-DG and 3-BP alone, 1 mM 2-DG and 100 μM 3-BP were added to cells, respectively. For 2-DG+PDT and 3-BP+PDT groups, cells were added 1 mM 2-DG or 100 μM 3-BP and then immediately exposed to PDT treatment. After various treatments, cells in the above groups were cultured for additional time as specified and subjected to different analyses.

2.5 Cytotoxicity assay

Rapid quantification of viable cells was performed with the Guava Viacount reagent (4000-0040; Millipore) which distinguishes between viable and nonviable cells on the basis of the differential permeability of DNA-binding dyes in the Viacount reagent and then provides absolute cell count and reliable determinations of viability data. This assay was performed exactly according to the manufacturer's instruction. Samples were analyzed by flow cytometry (Guava easyCyte 8HT, Millipore, Billerica,

MA).

2.6 Evaluating the interaction between 2-DG or 3-BP and PDT

Combination index (CI) was used to quantify the interaction between 2-DG/ 3-BP and PDT in this study. The CI was calculated by Jin's method.[20]

$$CI=E_{A+B} / (E_A + E_B - E_A \times E_B)$$

E_A or E_B was the effect of 2-DG/3-BP or PDT alone treatment group; E_{A+B} was the effect of the combined group with 2-DG/3-BP and PDT. A CI of >1 theoretically is a synergism. Considering experimental and statistical errors, a CI of 0.85-1.15 indicates an addition; a value of > 1.15 is a synergism and < 0.85 shows an antagonism.

2.7 Cell apoptosis detection

The ratio of apoptotic cells was measured with an Annexin V–FITC Apoptosis Detection Kit (Invitrogen, USA) according to the manufacturer's protocol. Briefly, at 24 h post different treatments, MDA-MB-231 cells and HUVEC were harvested and resuspended in 500 μl binding buffer, respectively. After adding 5 μl Annexin V–FITC and 5 μl PI into the cell suspension, the samples were incubated for 15 min at room temperature in the dark. The apoptotic index was immediately examined by flow cytometry (Millipore, Boston, MA, USA) and analyzed with FCS Express V3 software (DeNovo Software, Los Angeles, CA, USA).

2.8 Measurement of mitochondrial membrane potential (MMP)

RHO 123 can selectively enter into mitochondria with an intact membrane potential and is retained in the mitochondria. Once the mitochondrial membrane potential is lost, it cannot provide enough potential gradients for RHO123 to be absorbed and retained in the mitochondria.[21] At 6 h after different treatments, cells were washed by PBS, incubated with 1 μg/ml RHO 123 at 37 ℃ for 30 min, then resuspended with PBS and examined immediately by flow cytometry (Millipore, USA). Histograms were analyzed using FCS Express V3.

2.9 Immunofluorescence assay

After different treatments, cells were incubated with MTR in the dark at 37 ℃ for 15 min, then fixed with 4 % paraformaldehyde for 15 min. Subsequently, cells were permeabilized with 0.1 % Triton X-100 on ice for 5 min and blocked with normal goat serum at 37 ℃ for 1 h. After that, the samples were incubated with Bax antibody overnight at 4 ℃, and then were treated with the corresponding secondary antibodies (DyLightTM 594, FITC labeled) at 37 ℃ for 1 h. Finally, the cells were imaged with confocal laser scanning microscopy (TCS SP5 Leica, Wetzlar, Germany).

2.10 Western blot analysis

SDS–PAGE and immunoblotting were performed according to standard procedures. Briefly, after different treatments, cells were lysed in RIPA buffer on ice.

The protein samples were separated on a 12 % to 15 % SDS polyacrylamide gels, and then the proteins were transferred to PVDF membranes (Millipore, 0.22 μm pore size) and blotted with primary antibodies (caspase-3, Bax, Bcl-2, Phosphorylated P38 (Phospho-P38) and Phosphorylated JNK (Phospho-JNK)) overnight at 4 ℃. The bound primary antibodies were then tagged with IRDye 680 Conjugated IgG (Li-cor, Biosciences) at room temperature for 1 h. Infrared fluorescence was detected with the Odyssey infrared imaging system (Li-Cor Bioscience, Lincoln, NE). Anti-β-actin was used to ensure equal loading.

2.11 ROS detection and its role in cell death

Intracellular ROS production was studied by measuring the fluorescence intensity of dichlorofluorescein (DCF) as described in previous papers.[22] 2, 7-DCF-diacetate (DCFH-DA), a non- fluorescent cell permeant compound, is cleaved by endogenous esterases within the cell, and then the de-esterified product can be converted into the fluorescent compound DCF, upon oxidation by intracellular ROS. It has been reported the specificity of DCF is quite broad, with a spectrum including H^2O^2, $^{\cdot}OH$, $^{\cdot}O^{2-}$, $ONOO^-$, OCl^- and $^1O_2$,[23] which has been used as a common probe for intracellular ROS detection in PDT studies.[24-27] To estimate the intracellular ROS, we added 10 μM DCFH-DA before PDT treatment for 30 min. And at 0.5 h and 2 h post PDT treatment, cells were collected for DCF fluorescent detection.

To determine the role of ROS in cell death induced by the combined groups, the ROS scavenger NAC (5 mM) was added to culture medium prior to PDT treatment by 1

h, and then treated as described above.

2.12 Statistical analysis

All the experiments were performed in triplicate, and data were expressed as means ± SD. Differences between the each treated sample and control or the combined treated samples and PDT alone were assessed with SPSS software (SPSS, version 18.0). $p < 0.05$ was considered statistically significant, and $p < 0.01$ was extremely significant.

3. Results

3.1 Cytotoxicity of Ce6-PDT

In the presence of different Ce6 doses (0.5, 1, 2 and 4 μg/ml), the results of cell toxicity at 24 h after different treatments detected by the Guava Via-count reagent were shown in Figure 1. Live cells were on the left sides of the plot, while damaged cells were on the right. Figure 1A showed that in the dark, Ce6 alone didn't produce significant cytotoxicity. However, when exposed to 1.2 J/cm^2 light irradiation, PDT-induced cell damage was in a dose- dependent manner with the cytotoxicity increased from 8.1 ± 0.33 % (0.5 μg/ml Ce6-PDT) to 75.60 ± 3.09 % (4 μg/ml Ce6-PDT, $p < 0.01$, compared with control). 1 μg/ml of Ce6 might be a sensitive threshold for the PDT-induced cell damage on MDA-MB-231 cells (viable cells 78.2 ± 2.01 % in 1 μg/ml Ce6-PDT vs 95.7 ± 2.11 % in control, $p < 0.01$), and which was chosen for the subsequent analyses.

3.2 Cytotoxicity of the combined therapy with Ce6-PDT and 2-DG/3-BP

In the presence of different 2-DG dosages (0.5, 1 and 5 mM), the cell toxicity of MDA-MB-231 cells after PDT exposure (Ce6 dose=1 μg/ml, Light dose=1.2 J/cm^2) was plotted in Figure 1B. At 24 h post treatment, compared with the control, 2-DG alone didn't show significant cell damage from 1 mM to 5 mM. Whereas after combination with Ce6-PDT, a significant increase of cell toxicity could be observed in any 2-DG+PDT treatment group in a dose- dependent manner ($p < 0.01$, compared with 2-DG or PDT alone group). Similar results were observed in Figure 1C which showed the toxicity of cells after different 3-BP dosages (50, 100 and 200 μM) and PDT treatment group. 3-BP alone showed no significant inhibitory effect on MDA-MB-231 cells, while 3-BP+PDT could exert a significant cytotoxic effect with the survival rate decreased from 64.40 ± 1.71 % (50 μM, $p < 0.01$) to 28.40 ± 2.21 % (200 μM, $p < 0.01$), indicating a synergistic enhancement of cytotoxicity. As 1 mM 2-DG and 100 μM of 3-BP performed sensitivity to the efficacy of Ce6-PDT against MDA-MB-231 cells, we then adopted 1 mM 2-DG and 100 μM 3-BP combined with PDT to our subsequent analyses, respectively.

For comparison, HUVEC were used as normal cells to evaluate the cytotoxic anticancer activity of 2-DG/3-BP combined with PDT. Figure 1D showed that, compared with MDA-MB-231 cells, little cell damage was observed on HUVEC after 1 mM 2-DG+PDT and 100 μM 3-BP+PDT, suggesting the combination of 2-DG/3-BP and PDT has relatively selective tumor killing effect.

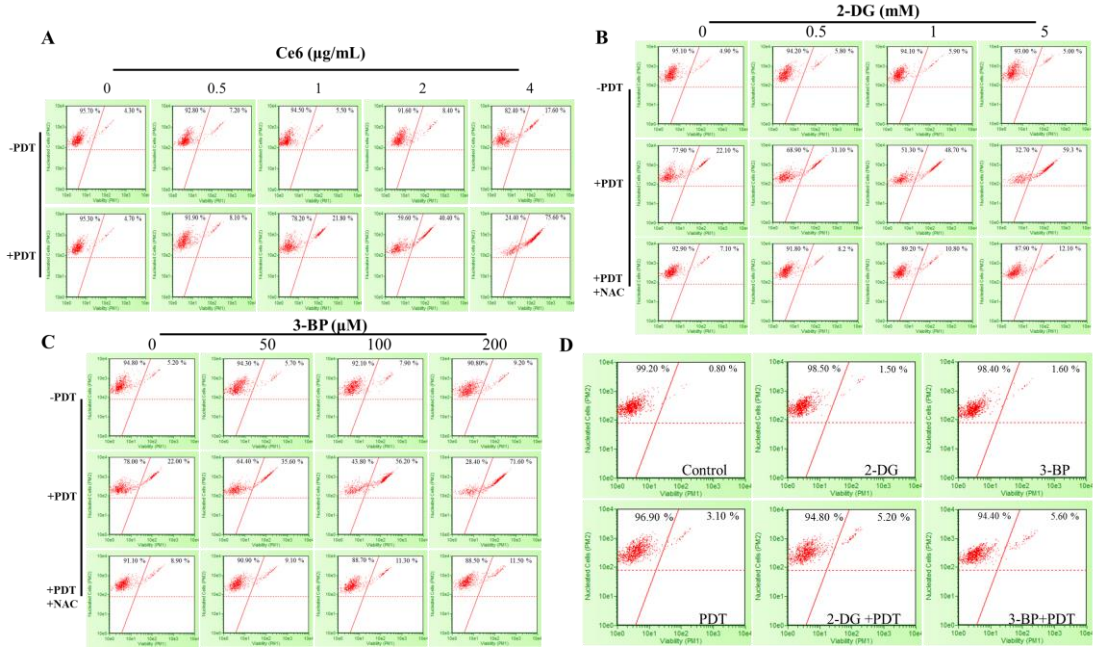

Figure 1. Effects of various treatments on the toxicity of MDA-MB-231 cells and HUVEC by via-count. A, MDA-MB-231 cells were treated with different concentrations of Ce6 (0.5, 1, 2 and 4 μg/ml) with (+) or without (-) 1.2 J/cm^2 light dose. **B,** MDA-MB-231 cells were treated with various concentrations of 2-DG (0.5, 1 and 5 mM) combined with (+) or without (-) 1 μg/ml Ce6-PDT. **C,** MDA-MB-231 cells were treated with different concentrations of 3-BP (50, 100 and 200 μM) combined with (+) or without (-) 1 μg/ml Ce6-PDT. **D,** HUVEC cytotoxicity was detected after different treatments. Control, no treatment; 2-DG, 1 mM 2-DG; 3-BP, 100 μM 3-BP; PDT, 1 μg/ml Ce6 + 1.2 J/cm^2 light dose; 2-DG+PDT, 1 mM 2-DG combined with 1 μg/ml Ce6-PDT; 3-BP+PDT, 100 μM 3-BP combined with 1 μg/ml Ce6-PDT. All data represent the means ± SD from triplicate separately.

3.3 The interaction between 2-DG/3-BP and PDT

1 mM 2-DG or 100 μM 3-BP was used to further analyze the combination effect

between 2-DG/3-BP and PDT. Cell damage effect was calculated from the data in Figure 1B and 1C:

$E_{2\text{-DG (0.5 mM)}} = 5.80 \pm 0.24$ % $E_{2\text{-DG (1 mM)}} = 5.90 \pm 0.23$ %, $E_{2\text{-DG (5 mM)}} = 5.00 \pm 0.20$ %;

$E_{PDT1} = 22.10 \pm 0.90$ %;

$E_{2\text{-DG (0.5 mM)+ PDT1}} = 31.10 \pm 1.27$ %, $E_{2\text{-DG (1mM)+ PDT1}} = 48.70 \pm 1.99$ %, $E_{2\text{-DG (5mM) + PDT1}} = 59.30 \pm 2.42$ %.

$E_{3\text{-BP (50 μM)}} = 5.70 \pm 0.23$ %, $E_{3\text{-BP (100 μM)}} = 7.90 \pm 0.32$ %, $E_{3\text{-BP (200 μM)}} = 9.20 \pm 0.38$ %;

$E_{PDT2} = 22.00 \pm 0.89$ %;

$E_{3\text{-BP (50 μM)} + PDT2} = 35.60 \pm 1.745$ %, $E_{3\text{-BP (100 μM)} + PDT2} = 56.20 \pm 2.29$ %, $E_{3\text{-BP (200 μM)} + PDT2} = 71.60 \pm 2.92$ %.

So based on $CI = E_{A+B} / (E_A + E_B - E_A \times E_B)$, we calculated that:

$CI_{2\text{-DG (0.5 mM)+PDT1}} = 1.16 \pm 0.51$, $CI_{2\text{-DG (1 mM)+PDT1}} = 1.82 \pm 0.70$, $CI_{2\text{-DG (5 mM)+PDT1}} = 2.28 \pm 0.93$;

$CI_{3\text{-BP (50 μM)} + PDT2} = 1.35 \pm 0.55$, $CI_{3\text{-BP (100 μM)} + PDT2} = 2.00 \pm 0.82$, $CI_{3\text{-BP (200 μM)} + PDT2} = 2.45 \pm 1.01$. As a CI value > 1.15 is a synergism, our results indicated that the interaction between 2-DG/3-BP and PDT were both synergisms (Figure 2).

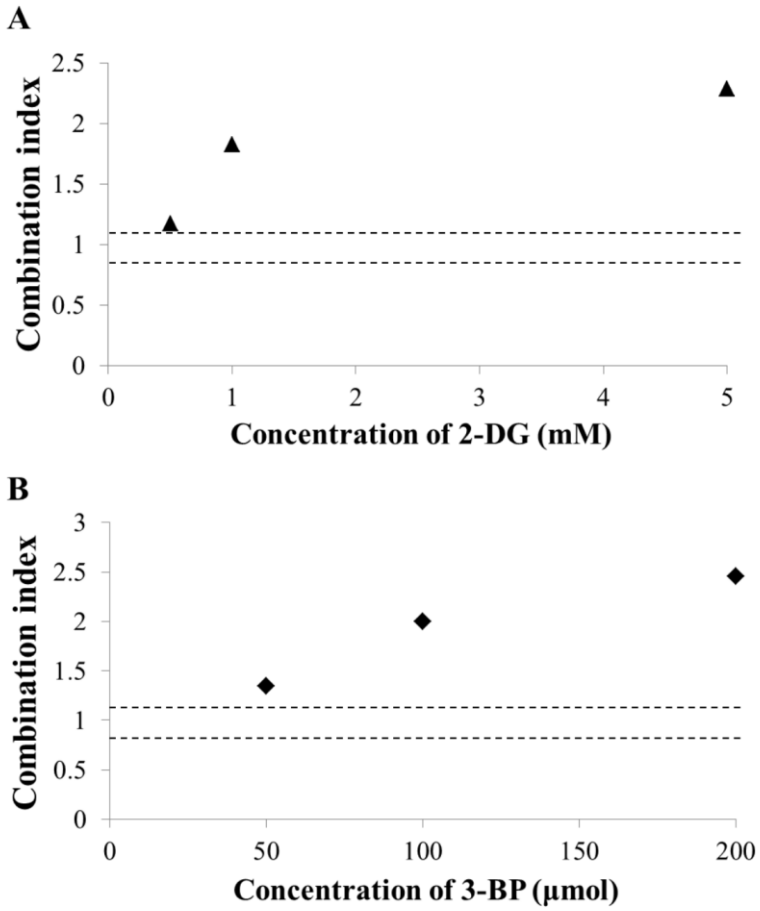

Figure 2. The combination indexes (CIs) of different concentrations of 2-DG/3-BP combined with PDT. The combination indexes (CIs) in (A) and (B) corresponded with the data in Figure 1B and 1C, respectively.

3.3 Cell apoptosis detection

To evaluate the apoptotic index induced by 2-DG/3-BP combined with PDT treatment, the Annexin V–FITC/PI double staining was performed at 24 h after different treatments. As plotted in Figure 3, the apoptotic cells (Annexin V-positive) in the control group were 2.25 ± 0.62 %; In the 2-DG and 3-BP alone groups, there were no apoptosis cells as well as in control; In the PDT treatment group, the apoptosis cells

possed 26.45 ± 1.02 %; While, in 2-DG+PDT and 3-BP+PDT treated groups, the proportion of Annexin V-positive cells were significantly increased to 45.15 ± 0.88 % and 50.35 ± 0.75 %, respectively. These results suggested that 2-DG and 3-BP significantly aggravated PDT-induced apoptosis in MDA-MB-231 cells.

While, non-malignant HUVEC did not show any significant increase in the Annexin V positive cells under the same treatment conditions with apoptosis rates of the 2-DG+PDT and 3-BP+PDT were 6.55 ± 0.35 % and 8.80 ± 0.52 % ($p > 0.05$, compared with control) (Figure 4).

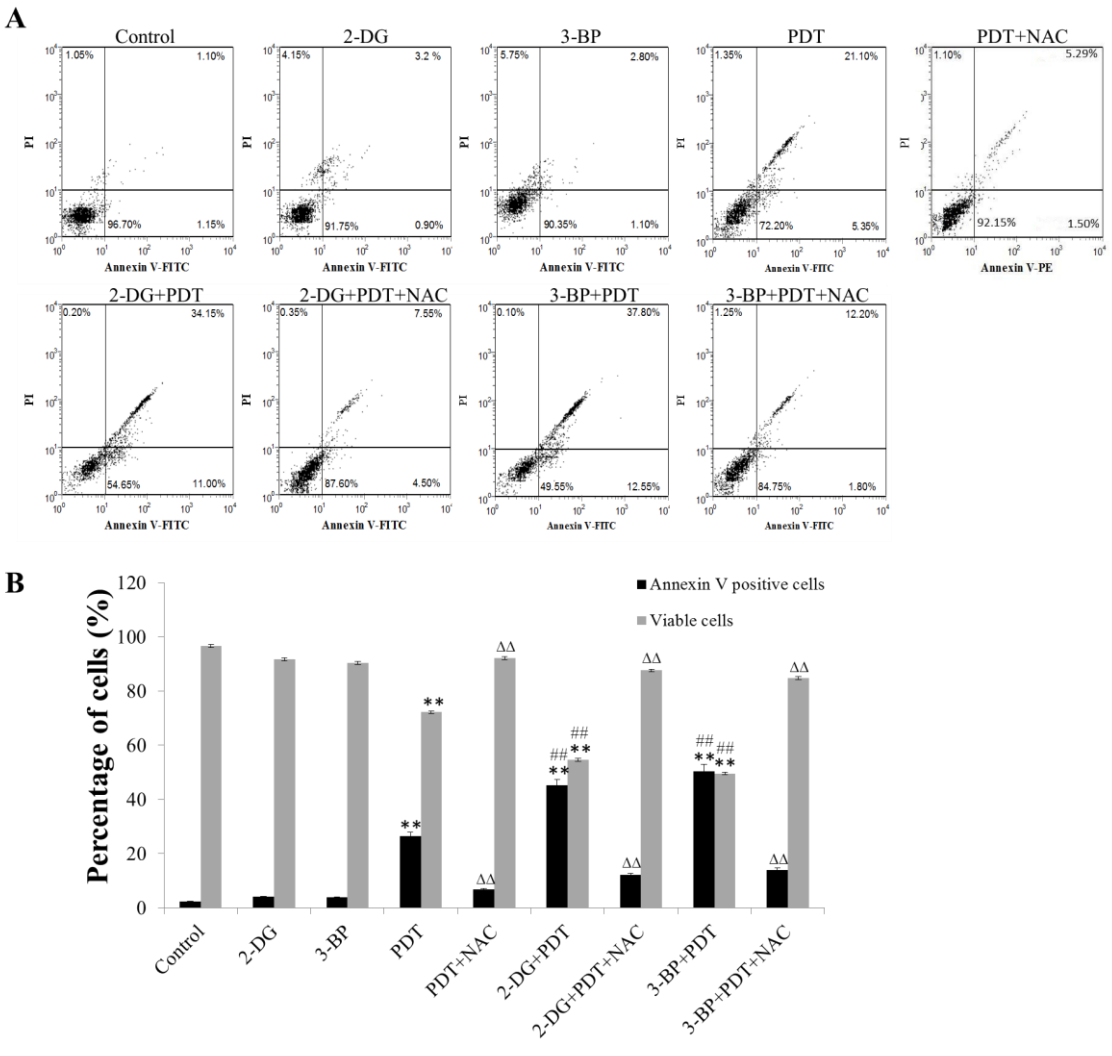

Figure 3. Apoptosis analysis using Annexin V-FITC/PI staining. A(a), Flow cytometric analysis of different treated cells induced apoptosis in MDA-MB-231 cells at 24 h. Control (untreated); 2-DG (1 mM); 3-BP (100 μM); PDT (1 μg/ml Ce6+1.2 J/cm^2 light dose); 2-DG+PDT (1 mM 2-DG combined with 1 μg/ml Ce6-PDT); 3-BP+PDT, (100 μM 3-BP combined with 1 μg/ml Ce6-PDT); PDT + NAC (1 μg/ml Ce6+1.2 J/cm^2 light dose+5 mM NAC); 2-DG+PDT+NAC, (1 mM 2-DG+1 μg/ml Ce6-PDT+5 mM NAC); 3-BP+PDT+NAC, (100 μM 3-BP+1 μg/ml Ce6-PDT+5 mM NAC). **B (b),** Histogram of viable cells and apoptotic cells at 24 h post treatment. Data shown are representative of three independent experiments. All data represent the means ± SD from triplicate separately. **$p < 0.01$ versus control, ##$p < 0.01$ versus PDT alone, ΔΔ$p < 0.01$ between with NAC and without NAC in each group.

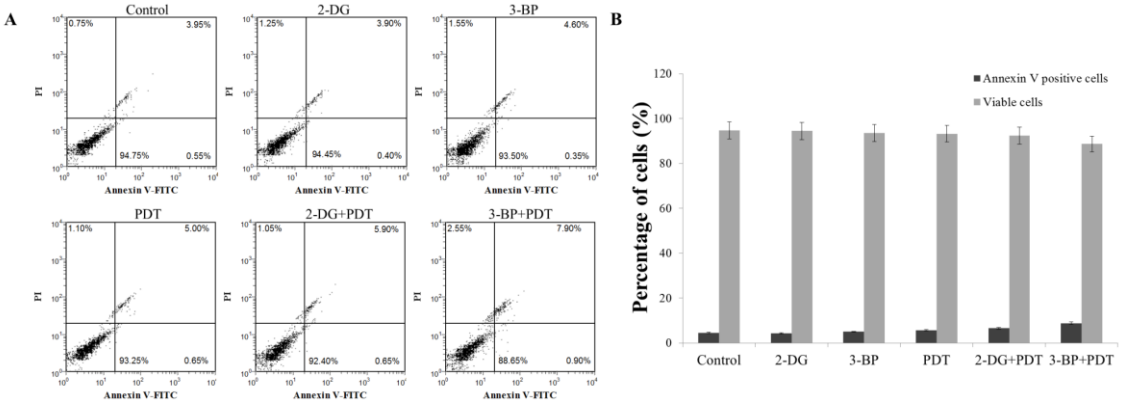

Figure 4. 2-DG+PDT and 3-BP+PDT induced apoptosis on HUVEC. A, Flow cytometric analysis of different treated cells induced apoptosis in HUVEC at 24 h. **B,** Histogram of viable cells and apoptotic cells at 24 h post-treatment. Data shown are representative of three independent experiments. All data represent the means ± SD from triplicate separately.

3.4 MMP detection

The flow cytometry combined with mitochondrial probe RHO123 was used to observe a decline in MMP after different treatments. As can be seen from Figure 5, compared with control group, the proportions of cells with MMP loss rose to 17.70 ± 1.21 % ($p < 0.01$) after being treated with PDT alone, whereas no obvious changes were detected in 2-DG/3-BP alone group. When treated with the combination of 2-DG/3-BP plus PDT, a more significant decline of MMP occurred (36.30 ± 1.57 % and 37.37 ± 1.57 %, respectively, $p < 0.01$).

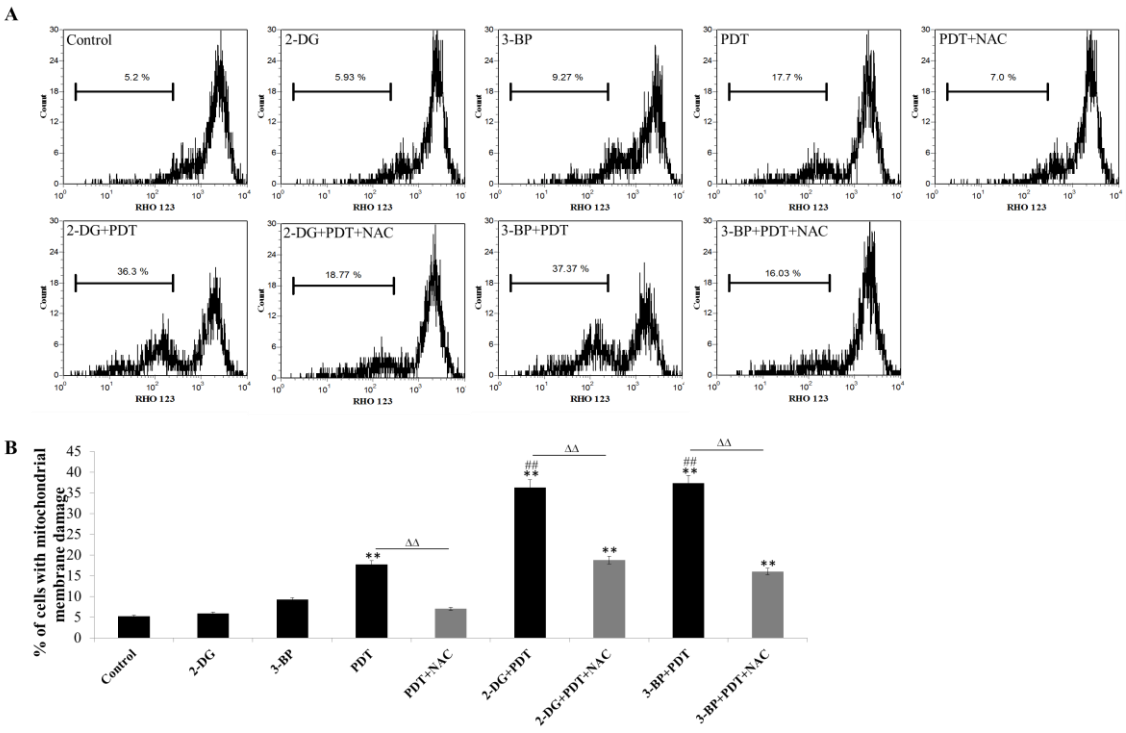

Figure 5. Detection of mitochondrial membrane potential (MMP) in MDA-MB-231 cells. A, Cells were stained with 1mg/ml RHO 123 and analyzed by flow cytometry at 6 h post treatment. **B**, Histogram of cells in MMP drop. Data shown are representative of three independent experiments. All data represent the means ± SD from triplicate separately. $^{**}p < 0.01$ versus control and $^{\#\#}p < 0.01$ versus PDT alone, $\Delta\Delta p < 0.01$ between with NAC and without NAC in each group.

3.5 Immunofluorescence staining

We detected relocalization of Bax to mitochondria after PDT alone and the combinations. Green was the Mito-Tracker Green fluorescent marker, red was the fluorescence emitted by Bax labeled by immunofluorescence staining (TRITC). Figure 6A showed cells with no significant co-localization between mitochondria and Bax in PDT alone at the detected time points, while cells in 2-DG+PDT group and 3-BP+PDT group showed obvious co-localization between mitochondria and Bax at 0.5 h post treatment. With the delayed incubations (at 1 h and 2 h post treatment), such co-localization phenomenon was not much obvious, suggesting that Bax translocation from cytoplasm to mitochondrion occurred in the early process of cell death to execute the pro-apoptotic response.

3.6 Expression changes of some key apoptosis related proteins

In the present study, we attempted to verify the changes of apoptosis-related proteins caspase-3, Bax and Bcl-2 by western blot after different treatments. Compared with PDT alone, 2-DG+PDT and 3-BP+PDT treated cells exhibited the increase of caspase-3 activity and decrease of Bcl-2 expression (Figure 6B), indicating an apoptotic response occurred in MDA-MB-231 cells following 2-DG/3-BP plus PDT treatment.

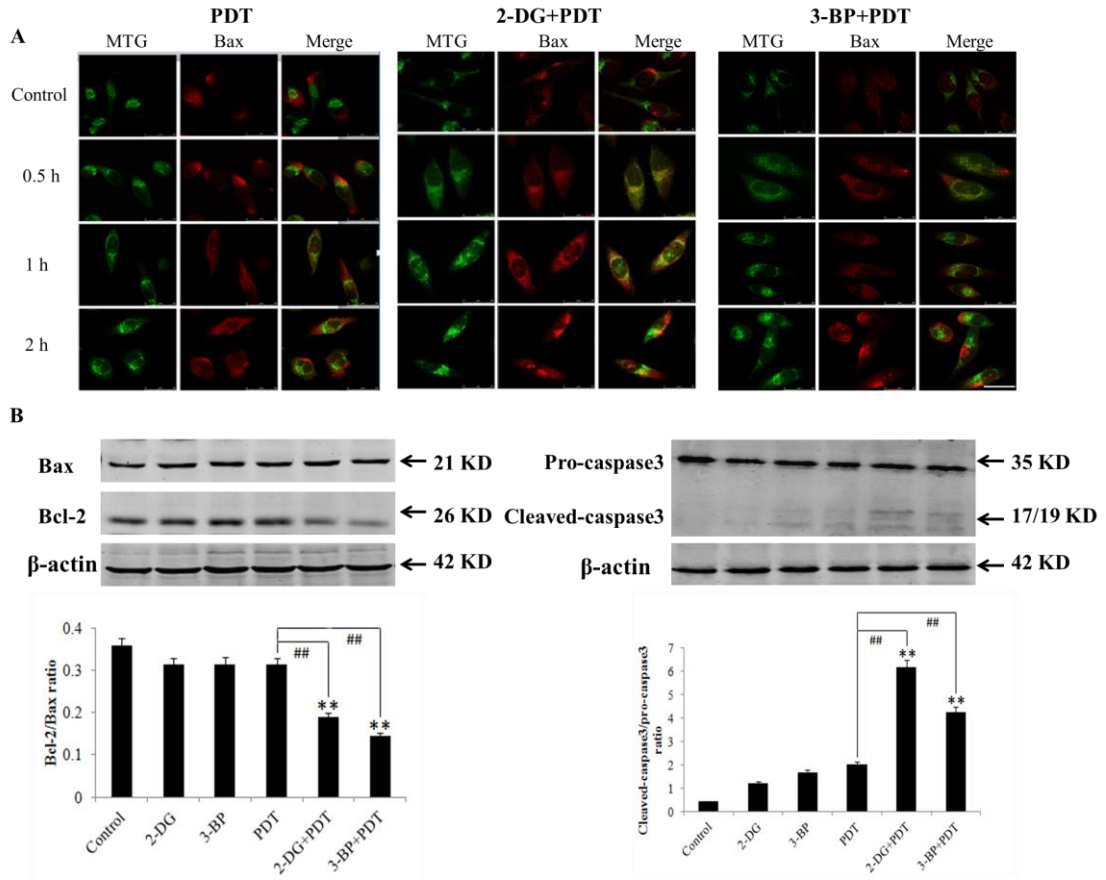

Figure 6. The co-localization between mitochondria and Bax and the activation of Bax/Bcl-2 and caspase-3 in 2-DG/3-BP+PDT treatment group. A, Cells in PDT alone, 2-DG+PDT and 3-BP+PDT groups were imaged with confocal laser scanning microscopy at different incubation times. **B,** Western blot analysis of Bax, Bcl-2, caspase-3 expression after different treatments. The ratios of Bcl-2/Bax and cleaved caspase-3/Procaspase-3 were statistically analyzed. All data represent the means ± SD from triplicate separately. Scale bar = 25 μm; **p* < 0.05 and ***p* < 0.01 versus Control, ##*p* < 0.01 versus PDT alone.

3.7 ROS detection and its role in protection of cell death

ROS have been shown to mediate the induction of apoptosis and ultimate cell fate.

Figure 7 showed that, compared with control, 49.30 ± 1.61 % of total cells displayed high DCF fluorescence in PDT alone, whereas 2-DG and 3-BP alone displayed no significant DCF fluorescence. More cells with such high fluorescence were observed when treated with 2-DG+PDT (94.93 ± 1.27 %, $p < 0.01$) after treatment for 0.5 h (Figure 7A). However, when the ROS levels of PDT and 2-DG+PDT groups recovered to 32.70 ± 1.33 % and 46.80 ± 1.91 % at 2 h post-treatment, respectively, 3-BP+PDT began to show relatively higher ROS levels (50.63 ± 2.06 %) than PDT alone ($p < 0.01$, Figure 7B).

In addition, the oxidative stress-associated proteins Phospho-P38 MAPK and P-JNK were analyzed by western blot. As shown in Figure 7C, compared with either monotherapy, increased phosphorylation of P38 and JNK were detected after 2-DG+PDT and 3-BP+PDT treatments, showing that an oxidative stress response occurred in MDA-MB-231 cells following the combinations. To further investigate the role of ROS in PDT induced cell death in MDA-MB-231 cells, cells were pre-treated with ROS scavenger NAC. The results in Figure 7A and 7B showed the intracellular ROS generations led by 2-DG+PDT and 3-BP+PDT treatments were both significantly blocked by NAC. In addition, 2-DG+PDT and 3-BP+PDT caused cell viability loss (Figure 1B and 1C), cell apoptosis (Figure 3B) and MMP drop (Figure 5) were all differently inhibited by NAC, suggesting ROS play a vital role in 2-DG+PDT and 3-BP+PDT induced apoptosis in MDA-MB-231 cells.

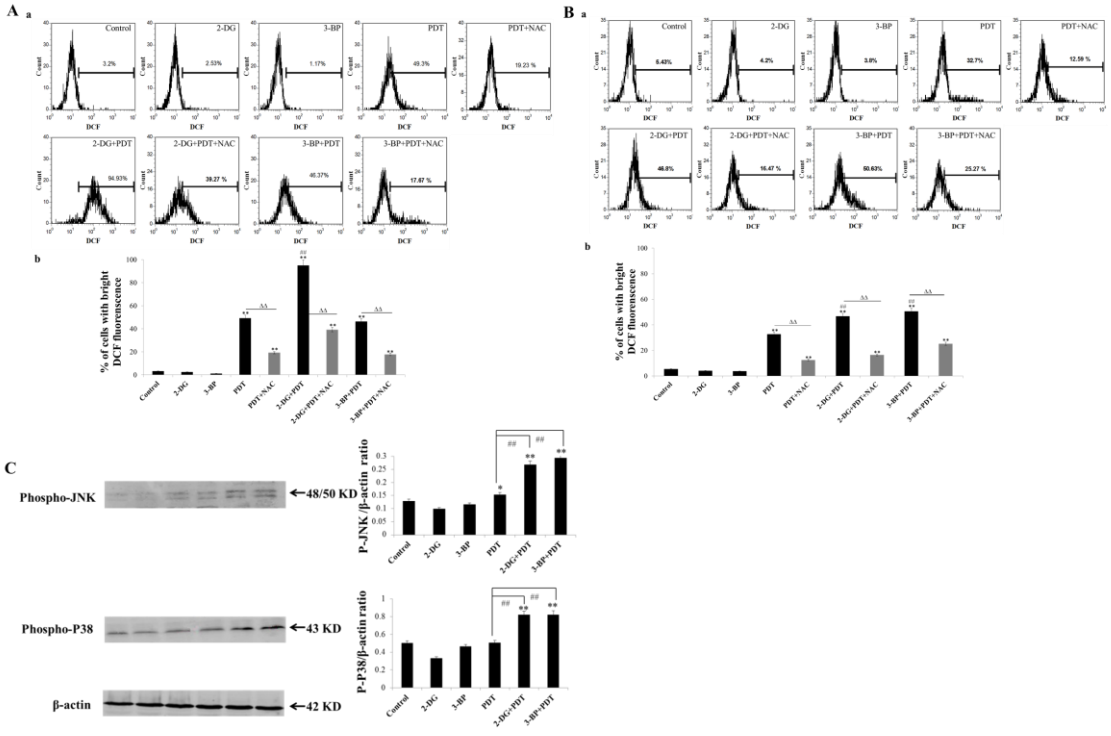

Figure 7. Measurement of intracellular ROS in MDA-MB-231 cells and the activation of MAPKs in 2-DG+PDT/3-BP+PDT treatment group. Cells were pre-incubated with DCFH-DA probe for 30 min before PDT treatment in various treatments. **A (a),** At 0.5 h post treatment, cells were collected for DCF fluorescent detection by flow cytometry. **A (b)**, Histogram of the ROS formation at 0.5 h post-treatment. **B (a),** At 2 h post treatment, cells were collected for DCF fluorescent detection by flow cytometry. **B (b)**, Histogram of the ROS formation at 2 h post-treatment. **C,** Western blot analysis of P-38 MAPK and JNK activation after different treatments. The ratios of P-JNK/β-actin and P-P38/β-actin were statistically analyzed. All data represent the means ± SD from triplicate separately. $^{**}p < 0.01$ versus control and $^{\#\#}p < 0.01$ versus PDT alone, $\Delta\Delta p < 0.01$ between with NAC and without NAC in each group.

Discussion

Results described here has demonstrated that aberrantly active glycolysis is required for malignant cells.[28] Therefore, aerobic glycolysis becomes an alternative strategy to achieve therapeutic selectivity to preferentially kill cancer cells.[29] Inhibition of glycolysis has been shown to enhance PDT mediated cytotoxicity in tumor cells,[19] but the potential mechanism remains unclear. Considering the significant differences among tumor cell lines, photosensitizer type, treatment protocols, radiation doses, etc., this study intended to investigate whether the general potentiation of PDT efficacy by 2-DG and 3-bromopyruvate (3-BP) could be observed on MDA-MB-231 cells and why these phenomena occurred.

When determining the cytotoxicity of Ce6 alone, an initial drug dosage- dependent manner on cell survival rate was observed in Figure 1A. It showed that cell toxicity varied with different doses of Ce6 at a given light dose (1.2 J/cm^2, Figure 1A). Therein, PDT triggered moderate cellular damage at a chosen Ce6 dose of 1 μg/ml and was used for the subsequent analyses.

With the introduction of glycolysis inhibitors into the PDT field, a remarkable increase of PDT induced cytotoxicity was observed with the presence of 2-DG (Figure 1B, $p < 0.01$, compared with control, 2-DG or PDT alone). Similarly, 3-BP could also significantly enhance the cytotoxicity of PDT in a dose-dependent manner (Figure 1C). HUVEC showed little cell damage under the same treated conditions ($p < 0.01$, Figure 1D). Meanwhile, CIs indicated synergisms between 2-DG/3-BP and PDT (Figure 2),

which show the PDT efficacy could be greatly enhanced by glycolysis inhibitors. This was in accordance with Golding's report.[19]

Apoptosis is currently viewed as the most important death modality involving a series of typical features.[30] Subsequently, the apoptotic rate of different treatment groups were evaluated by Annexin V-FITC/PI double staining. Our results suggested at the given experimental conditions, the combination of 2-DG/3-BP and PDT could significantly increase the ratio of apoptosis in MDA-MB-231 cells (45.15 ± 0.88 % in 2-DG+PDT group and 50.35 ± 0.75 % in 3-BP+PDT group versus 4.1± 0.94 % in 2-DG, 3.9 ± 0.68 % in 3-BP, and 26.45±1.02 % in PDT, $p < 0.01$). The results indicate the interaction between 2-DG/3-BP and PDT could achieve a synergism under our experimental conditions. In contrast, no significant cell apoptosis was observed on HUVEC (Figure 4), implying the cytotoxic effect of the combined treatment might mainly target cancer cells and trigger cellular apoptotic response.

In PDT treatment, mitochondria tend to be the initially vulnerable site where Ce6 mainly located.[31] Besides, 2-DG and 3-BP both can inactivate HK-II and dissociates the enzyme from the mitochondria, which eventually triggers apoptosis.[32] In view of that, we investigated whether mitochondria was the main target for the combinations mediated cell apoptosis under our experimental conditions. Evidence obtained in this study showed an obvious drop in MMP after treatment with 2-DG+PDT and 3-BP+PDT when compared with either monotherapy (Figure 5), suggesting the MMP drop may act as a sensitive indicator of cell injury after these combined therapies.

Bcl-2 family proteins play important roles in regulation of mitochondria linked apoptosis.[33] Bax, as an important member of Bcl-2 subfamilies, is pro-apoptotic protein, while Bcl-2 is an anti-apoptotic factor.[34] As the immunofluorescence analysis revealed, after 2-DG+PDT and 3-BP+PDT treatments, Bax redistribution was prominent and time dependent (Figure 6A). Further, western blot showed that the Bcl-2 protein was highly expressed in each monotherapy, (Figure 6B), while its expression significantly decreased in 2-DG+PDT and 3-BP+PDT groups, illustrating that the combinations promoted cell apoptosis through down-regulating the expression of anti-apoptotic Bcl-2 protein. Caspases play central roles in apoptosis. Caspase-3 is the major downstream effector of caspases and is usually activated by various death signals and can cleave important cellular proteins.[35] Obtained data indicated that caspase-3 activity was also obviously increased in the combined groups (Figure 6B). These results suggested that mitochondrial- and caspase- dependent cell apoptosis pathways were closely associated with cell death induced by 2-DG+PDT and 3-BP+PDT.

PDT-induced oxidative stress is one of the major initiators of cell death[36] and also can be caused by glucose deprivation.[37] In our study, we found a rapid generation of intracellular ROS in PDT group, whereas there was no obvious occurrence in the control and 2-DG/3-BP alone groups. Moreover, the yields of ROS in 2-DG+PDT and 3-BP+PDT groups were much higher than PDT alone with significant time-dependent sequential (Figure 7A and 7B). Mitogen-activated protein kinase (MAPK) signal pathways are usually responsible for ROS-mediated cell apoptosis.[38] Therein, JNK

activation is usually associated with apoptosis induction[39] and P38 MAPK relates to pro-apoptosis or anti-apoptosis, which depends on the specific stimulus and cell type.[40] Expectedly, in the current study, we observed that the phosphorylation of P38 and JNK were enhanced by 2-DG+PDT and 3-BP+PDT, compared with PDT alone (Figure 7C). These data suggested that oxidant injury, which elicits a wide spectrum of responses such as growth arrest, cell death, etc., might be involved in response to the combination of glycolysis inhibitors and PDT in MDA-MB-231 cells.

Yet for all that, our present results were somewhat inconsistent with Golding's report.[19] Golding has assayed the ROS levels after different treatments with adding 180 mM 2-DG or 300 μM lonidamine immediately post PDT for different time. Under their experimental conditions, they report that 2-DG gives lower DCF fluorescence readings than PDT over the same time course but lonidamine shows higher ROS production than PDT at the time post-treatment (< 210 min). While, in our experiments, 2-DG (1 mM) and 3-BP (100 μM) were added 15 min before PDT and then maintained for different time period for the subsequent experiments. Results indicated both of 2-DG/3-BP can aggravate ROS production induced by PDT, showing a significant time-dependent sequential. And, there might be a great deal of uncertainty due to intrinsic differences between cell types and the different time of glycolytic inhibitors exposure. Vibhuti has studied head and neck carcinoma cells, which bear mutations in p53, were more susceptible to glycolytic inhibitor-induced cytotoxicity possibly due to enhanced metabolic oxidative stress mediated by 2-DG linked to mutations in p53.[41]

Coincidentally, we used human breast cancer MDA-MB-231 cells which are p53 mutations and Golding has used MCF-7 cells which are P53 wild-type. These might be one of reasons why we reported a significant increase in ROS accumulation with 2-DG+PDT while Golding did not under distinct conditions.

Additionally, co-administration with NAC (a special ROS scavenger), the ROS generation (Figure 7A and 7B), MMP drop (Figure 5), cell apoptotic (Figure 3) and cytotoxicity (Figure 1B-C) were differently relieved, implying an oxidative stress mechanism may be involved in response to 2-DG/-BP plus PDT in MDA-MB-231 cells.

Although ROS was a key component during 2-DG+PDT and 3-BP+PDT treatments in our experiment, other factors may also simultaneously exist. Jain has reported that the presence of 2-DG following irradiation could inhibit DNA repair and cellular recovery processes selectively in cancer cells leading to enhanced radiation damage, while sparing in normal cells.[42] Further, 2-DG has been shown to selectively deplete ATP and could enhance autophagy-triggered cell death.[43, 44] 3-BP is found to inhibit the membrane potential, oxygen consumption, dehydrogenase activities, global protein synthesis and further contributing to cancer cell death.[45, 46] So, the potential mechanisms whereby glycolysis inhibitors enhanced PDT efficacy were complex and multifactorial and needed further deep investigations.

To sum up, the presented results indicated that: (i) The presence of 1 mM 2-DG and 100 μM 3-BP were shown to greatly improve the cytotoxicity of Ce6-PDT on MDA-MB-231 human breast cancer cells; (ii) 2-DG+PDT and 3-BP+PDT could induce

mitochondrial- and caspase- dependent apoptosis in MDA-MB-231 cells; (iii) ROS played a vital role in the enhanced cell apoptosis in these combined treatments.

Conflict of interest

There are no conflicts of interest to declare.

Acknowledgments

This work was supported by the National Natural Science Foundation of China (Grant No. 81472846), the China Postdoctoral Science Foundation (Grant No. 2014M550477), the Natural Science Foundation of Shaanxi Province, China (Grant No. 2014JQ3092) and the Fundamental Research Funds for the Central Universities (GK201302022).

Reference

1. N. Hammoudi, K. B. Ahmed, C. Garcia-Prieto and P. Huang, The Warburg effect and its cancer therapeutic implications, *Chin J Cancer*., 2011, **30**, 508-525.
2. M. G. Vander Heiden, L. C. Cantley and C. B. Thompson, Understanding the Warburg effect: themetabolic requirements of cell proliferation, *Science*., 2009, **324**, 1029-1033.
3. L. Galluzzi, O. Kepp, M. G. Vander Heiden and G. Kroemer, Metabolic targets for cancer therapy, *Nat. Rev. Drug Disc*., 2013, **12**, 829-846.
4. C. Granchi and F. Minutolo, Anticancer Agents That Counteract Tumor Glycolysis, *Chem Med Chem*., 2012, **7**, 1318-1350.
5. T. N. Seyfried, R. E. Flores, A. M. Poff and D. P. D'Agostino, Cancer as a

Metabolic Disease: Implications for Novel Therapeutics, *Carcinogenesis*., 2014, **35**(3), 515-27.

6. L. P. Peter, Warburg, me and Hexokinase 2: Multiple discoveries of key molecular events underlying one of cancers' most common phenotypes, the"Warburg Effect", i.e., elevated glycolysis in the presence of oxygen, *J Bioenerg Biomembr*., 2007, **39**, 211–222.

7. P. M. Saroj, H. K. Young and L. P. Peter, Hexokinase-2 bound to mitochondria: Cancer's stygian link to the"Warburg effect" and a pivotal target for effective therapy, *Semin Cancer Biol*., 2009, **19**, 17–24.

8. E. Hulleman, K. M. Kazemier, A. Holleman, D. J. VanderWeele, C. M. Rudin, M. J. Broekhuis, W. E. Evans, R. Pieters and M. L. Den Boer, Inhibition of glycolysis modulates prednisolone resistance in acute lympho blastic leukemia cells, *Blood*., 2009, **113**, 2014 21.

9. D. Trachootham, J. Alexandre and P. Huang, Targeting cancer cells by ROS-mediated mechanisms: a radical therapeutic approach? *Nat Rev Drug Discov*., 2009, **8**, 579–591.

10. B. S. Dwarakanath, D. Singh, A. K. Banerji, R. Sarin, N. K. Venkataramana, R. Jalali, P. N. Vishwanath, B. K. Mohanti, R. P. Tripathi, V. K. Kalia and V. Jain, Clinical studies for improving radiotherapy with 2-deoxy-D-glucose: present status and future prospects, *J Cancer Res Ther*., 2009, **1**, S21-6.

11. H Pelicano1, DS Martin2, R-H Xu and P Huang, Glycolysis inhibition for

anticancer treatment, *Oncogene*., 2006, **25**, 4633–4646.

12. G. Maschek, N. Savaraj, W. Priebe, P. Braunschweiger, K. Hamilton, G. F. Tidmarsh, L. R. De Young and T. J. Lampidis, 2-Deoxy-D-glucose increases the efficacy of adriamycin and paclitaxel in human osteosarcoma and non-small cell lung cancers in vivo, *Cancer Res*., 2004, **64**, 31-34.
13. L. S. Ihrlund, E. Hernlund, O. Khan and M. C. Shoshan, 3-Bromopyruvate as inhibitor of tumour cell energy metabolism and chemopotentiator of platinum drugs. *Mol Oncol*., 2008, **2**, 94-101.
14. P. Agostinis, K. Berg, K. A. Cengel, T. H. Foster, A. W. Girotti, S. O. Gollnick, S. M. Hahn, M. R. Hamblin, A. Juzeniene, D. Kessel, M. Korbelik, J. Moan, P. Mroz, D. Nowis, J. Piette, B. C. Wilson and J. Golab, Photodynamic therapy of cancer: An update, *CA Cancer J Clin*., 2011, **61**, 250–281.
15. S. Anand, B. J. Ortel, S. P. Pereira, T. Hasan and E. V. Maytin, Biomodulatory approaches to photodynamic therapy for solid tumors. *Cancer Lett*., 2012, **326**, 8–16.
16. S. G. Bown, How mainstream medicine sees photodynamic therapy in the United Kingdom, *J Natl Compr Canc Netw*., 2012, **10**, S69–S74.
17. L. M. Davids and B. Kleemann, Combating melanoma: The use of photodynamic therapy as a novel, adjuvant therapeutic tool, *Cancer Treat Rev*., 2011, **37**, 465-475.
18. E. Crescenzi, A. Chiaviello, G. Canti, Low doses of cisplatin or gemcitabine

plus Photofrin/photodynamic therapy: Disjointed cell cycle phase-related activity accounts for synergistic outcome in metastatic non-small cell lung cancer cells (H1299), *Mol Cancer Ther*., 2006, **5**, 776-785.

19. J. P. Golding, T. Wardhaugh, L. Patrick, M. Yurner, J. B. Phillips, J. I. Bruce and S. G. Kimani, Targeting tumour energy metabolism potentiates the cytotoxicity of 5-aminolevulinic acid photodynamic therapy, *British Journal of Cancer*., 2013, **109**(4), 976–982.

20. Z. J. Jin's, About the evaluation of drug combination. *Acta Pharmacol Sin*, 2004, **25**, 146-147.

21. X. Wang, Q. Liu, P. Wang, Z. Wang, W. Tong, B. Zhu, Y. Wang and C. Li, Comparisons among sensitivities of different tumor cells to focused ultrasoundin vitro, *Ultrasonics*., 2009, **49**, 558e564.

22. Y. Li, P. Wang, P. Zhao, S. Zhu, X. Wang and Q. Liu, Apoptosis induced by sonodynamic treatment by protoporphyrin IX on MDA-MB-231 cells, *Ultrasonics*., 2012, **52**, 490-496.

23. D. Kessel and J Jr. Reiners, Light-Activated Pharmaceuticals: Mechanisms and Detection, *Isr J Chem*., 2012, **52**, 674–680.

24. B. Wang, J. Wang, Q. Liu, H. Huang, M. Chen, K. Li, C. Li, X. Yu and P. Chu, Rose-bengal-conjugated gold nanorods for in vivo photodynamic and photothermal oral cancer therapies, *Biomaterials*., 2014, **35**, 1954-1966.

25. N. Rubio, J. Verrax, M. Dewaele, T. Verfaillie, T. Johansen, J. Piette and P.

Agostinis, p38(MAPK)-regulated induction of p62 and NBR1 after photodynamic therapy promotes autophagic clearance of ubiquitin aggregates and reduces reactive oxygen species levels by supporting Nrf2-antioxidant signaling, *Free Radic Biol Med*., 2014, **67**, 292-303.

26. C. Kim, C. Chung, K. Choi, J. Yoo, D. Kim, Y. Jeong and D Kang, Effect of 5-aminolevulinic acid-based photodynamic therapy via reactive oxygen species in human cholangiocarcinoma cells, *Int J Nanomedicine*., 2011, **6**, 1357-1363.
27. P. He, J. Ahn, I. Shin and P. Chung, Photoactivation of 9-hydroxypheophorbide alpha triggers apoptosis through the reactive oxygen species-mediated mitochondrial pathway and endoplasmic reticulum stress in AMC-HN-3 laryngeal cancer cells, *Int J Oncol*., 2010, **36**, 801-808.
28. H. Pelicano, D. S. Martin, R. H. Xu and P. Huang, Glycolysis inhibition for anticancer treatment, *Oncogene*., 2006, **25**, 4633-4646.
29. M. Cuperlovic-Culf, A. Culf, M. Touaibia and N. Lefort, Targeting the latest hallmark of cancer: another attempt at 'magic bullet' drugs targeting cancers' metabolic phenotype, *Future Onco*., 2012, **l8**, 1315–1330.
30. S. Rello, J. C. Stockert, V. Moreno, A. Gámez, M. Pacheco, A. Juarranz, M. Cañete and A. Villanueva, Morphological criteria to distinguish cell death induced by apoptotic and necrotic treatments, *Apoptosis*., 2005, **10**, 201–208.
31. H. P. Wang, X. B. Wang, P. Wang, K. Zhang, S. Yang and Q. H. Liu, Ultrasound enhances the efficacy of Chlorin e6-mediatedphotodynamic therapy in

MDA-MB-231 cells, *Ultrasound in Med. & Biol*., 2013, **19**, 1713–1724.

32. K. K. Arora and P. L. Pedersen, Functional significance of mitochondrial bound hexokinase in tumor cell metabolism. Evidence for preferential phosphorylation of glucose by intramitochondrially generated ATP, *J Biol Che*., 1988, **263**, 17422–8.

33. A. M. Petros, A. Medek, D. G. Nettesheim, D. H. Kim, H. S. Yoon, K. Swift, E. D. Matayoshi, T. Oltersdorf, S. W. Fesik, Solution structure of the antiapoptotic protein BCL-2, *Proc. Natl. Acad. Sci. USA*., 2001, **98**(6), 3012–3017.

34. T. Kuwana, M. R. Mackey, G. Perkins, M. H. Ellisman, M. Latterich, R. Schneiter, D. R. Green and D. D. Newmeyer, BAX and lipids cooperate to form supramolecular openings in the outer mitochondrial membrane, *Cell*., 2002, **111**(3), 331–342.

35. A. G. Porter and R. U. Janicke, Emerging roles of caspase-3 in apoptosis, *Cell Death Differ*., 1999, **6**(2), 99–104.

36. R. Hilf, R. S. Murant, U. Narayanan and S. L. Gibson, Relationship of Mitochondrial Function and Cellular Adenosine Triphosphate Levels to Hematoporphyrin Derivative-induced Photosensitization in R3230AC Mammary Tumors, *Cancer Res*., 1986, **46**, 211-217.

37. K. Tobias, P. Kristjan, B. O. Christian, B. Juergen, J. O. Franz and K. Barbara, Differential effects of glucose deprivation on the cellular sensitivity towards

photodynamic treatment-based production of reactive oxygen species and apoptosis-induction, *FEBS Letters*., 2005, **579**, 185–190.

38. A. Matsuzawa and H. Ichijo, Stress-responsive protein kinases in redox-regulated apoptosis signaling. Antioxidants & Redox Signaling., 2005, 7, 472–481.

39. V. Temkin and M. Karin, From death receptor to reactive oxygen species and c-Jun N-terminal protein kinase: The receptor-interacting protein 1 odyssey, *Immunological Reviews*., 2007, **220**, 8–21 .

40. Y. M. Ha, M. K. Park, H. J. Kim, H. G. Seo, J. H. Lee and K. C. Chang, High concentrations of ascorbic acid induces apoptosis of human gastric cancer cell by p38-MAP kinase-dependent up-regulation of transferrin receptor, *Cancer Lett*., 2009, **277**, 48-54.

41. A. Vibhuti, K. Muralidhar and B. S. Dwarakanath, Differential cytotoxicity of the glycolytic inhibitor 2-deoxy-D-glucose in isogenic cell lines varying in their p53 status, *J Cancer Res Ther*., 2013, **9**(4), 686-92.

42. V. Jain, Modifications of radiation responses by 2-deoxy-D-glucose in normal and cancer cells, *Ind. J. Nucl. Med*., 1996, **11**, 8–17.

43. H. Xi, J. C. Barredo, J. R. Merchan and T. J. Lampidis, Endoplasmic reticulum stress induced by 2-deoxyglucose but not glucose starvation activates AMPK through CaMKKβ leading to autophagy, *Biochemical Pharmacology*., 2013, **85**(10), 1463-77.

44. Q. Wang, B. Liang, N. A. Shirwany and M. H. Zou, 2-Deoxy-D-glucose treatment of endothelial cells induces autophagy by reactive oxygen species-mediated activation of the AMP-activated protein kinase, *PLoS On*e., 2011, **6**(2), e17234.

45. C. Rodrigues-Ferreira, A. P. da Silva and A. Galina, Effect of the antitumoral alkylating agent 3-bromopyruvate on mitochondrial respiration: role of mitochondrially bound hexokinase, *J Bioenerg Biomembr*., 2012, **44**(1), 39-49.

46. S. Ganapathy-Kanniappan, M. Vali, R. Kunjithapatham, M. Buijs, L. H. Syed, P. P. Rao, S. Ota, B. K. Kwak, R. Loffroy and J. F. Geschwind, 3-bromopyruvate: a new targeted antiglycolytic agent and a promise for cancer therapy, *Curr Pharm Biotechnol*., 2010, **11**(5), 510-7.

Figure legends

Figure 1. Effects of various treatments on the toxicity of MDA-MB-231 cells and HUVEC by via-count. A, MDA-MB-231 cells were treated with different concentrations of Ce6 (0.5, 1, 2 and 4 μg/ml) with (+) or without (-) 1.2 J/cm^2 light dose. **B,** MDA-MB-231 cells were treated with various concentrations of 2-DG (0.5, 1 and 5 mM) combined with (+) or without (-) 1 μg/ml Ce6-PDT. **C,** MDA-MB-231 cells were treated with different concentrations of 3-BP (50, 100 and 200 μM) combined with (+) or without (-) 1 μg/ml Ce6-PDT. **D,** HUVEC cytotoxicity was detected after different treatments. Control, no treatment; 2-DG, 1 mM 2-DG; 3-BP, 100 μM 3-BP; PDT, 1 μg/ml Ce6 + 1.2 J/cm^2 light dose; 2-DG+PDT, 1 mM 2-DG combined with 1 μg/ml Ce6-PDT; 3-BP+PDT, 100 μM 3-BP combined with 1 μg/ml Ce6-PDT. All data represent the means ± SD from triplicate separately.

Figure 2. The combination indexes (CIs) of different concentrations of 2-DG/3-BP combined with PDT. The combination indexes (CIs) in (A) and (B) corresponded with the data in Figure 1B and 1C, respectively.

Figure 3. Apoptosis analysis using Annexin V-FITC/PI staining. A(a), Flow cytometric analysis of different treated cells induced apoptosis in MDA-MB-231 cells at 24 h. Control (untreated); 2-DG (1 mM); 3-BP (100 μM); PDT (1 μg/ml Ce6+1.2 J/cm^2 light dose); 2-DG+PDT (1 mM 2-DG combined with 1 μg/ml Ce6-PDT); 3-BP+PDT, (100 μM 3-BP combined with 1 μg/ml Ce6-PDT); PDT + NAC (1 μg/ml Ce6+1.2 J/cm^2 light dose+5 mM NAC); 2-DG+PDT+NAC, (1 mM 2-DG+1 μg/ml Ce6-PDT+5 mM

NAC); 3-BP+PDT+NAC, (100 μM 3-BP+1 μg/ml Ce6-PDT+5 mM NAC). **B (b),** Histogram of viable cells and apoptotic cells at 24 h post treatment. Data shown are representative of three independent experiments. All data represent the means ± SD from triplicate separately. $^{**}p < 0.01$ versus control, $^{\#\#}p < 0.01$ versus PDT alone, $^{\Delta\Delta}p < 0.01$ between with NAC and without NAC in each group.

Figure 4. 2-DG+PDT and 3-BP+PDT induced apoptosis on HUVEC. A, Flow cytometric analysis of different treated cells induced apoptosis in HUVEC at 24 h. **B,** Histogram of viable cells and apoptotic cells at 24 h post-treatment. Data shown are representative of three independent experiments. All data represent the means ± SD from triplicate separately.

Figure 5. Detection of mitochondrial membrane potential (MMP) in MDA-MB-231 cells. A, Cells were stained with 1mg/ml RHO 123 and analyzed by flow cytometry at 6 h post treatment. **B**, Histogram of cells in MMP drop. Data shown are representative of three independent experiments. All data represent the means ± SD from triplicate separately. $^{**}p < 0.01$ versus control and $^{\#\#}p < 0.01$ versus PDT alone, $^{\Delta\Delta}p < 0.01$ between with NAC and without NAC in each group.

Figure 6. The co-localization between mitochondria and Bax and the activation of Bax/Bcl-2 and caspase-3 in 2-DG/3-BP+PDT treatment group. A, Cells in PDT alone, 2-DG+PDT and 3-BP+PDT groups were imaged with confocal laser scanning microscopy at different incubation times. **B,** Western blot analysis of Bax, Bcl-2, caspase-3 expression after different treatments. The ratios of Bcl-2/Bax and cleaved

caspase-3/Procaspase-3 were statistically analyzed. All data represent the means ± SD from triplicate separately. Scale bar = 25 μm; *$p < 0.05$ and **$p < 0.01$ versus Control, ##$p < 0.01$ versus PDT alone.

Figure 7. Measurement of intracellular ROS in MDA-MB-231 cells and the activation of MAPKs in 2-DG+PDT/3-BP+PDT treatment group. Cells were pre-incubated with DCFH-DA probe for 30 min before PDT treatment in various treatments. **A (a),** At 0.5 h post treatment, cells were collected for DCF fluorescent detection by flow cytometry. **A (b)**, Histogram of the ROS formation at 0.5 h post-treatment. **B (a),** At 2 h post treatment, cells were collected for DCF fluorescent detection by flow cytometry. **B (b)**, Histogram of the ROS formation at 2 h post-treatment. **C,** Western blot analysis of P-38 MAPK and JNK activation after different treatments. The ratios of P-JNK/β-actin and P-P38/β-actin were statistically analyzed. All data represent the means ± SD from triplicate separately. **$p < 0.01$ versus control and ##$p < 0.01$ versus PDT alone, $\Delta\Delta p < 0.01$ between with NAC and without NAC in each group.